

The dynamics of starvation and recovery

2 Justin D. Yeakel * †‡, Christopher P. Kempes †, and Sidney Redner †§

3 *School of Natural Science, University of California Merced, Merced, CA, †The Santa Fe Institute, Santa Fe, NM, §Department of Physics, Boston University, Boston
4 MA, and ‡To whom correspondence should be addressed: jdyeakel@gmail.com

5 Submitted to Proceedings of the National Academy of Sciences of the United States of America

6 The eco-evolutionary dynamics of species is fundamentally linked
7 to the energetic constraints of its constituent individuals. Of par-
8 ticular importance are the tradeoffs between reproduction and
9 the dynamics of starvation and recovery in resource-limited envi-
10 ronments. To elucidate the consequences of this tradeoff, we
11 introduce a minimal nutritional state-structured model that in-
12 corporates two classes of consumer: nutritionally replete con-
13 sumers that reproduce, and undernourished, non-reproducing
14 consumers that are susceptible to mortality. As a function of the
15 transition rates between these replete and undernourished states
16 that are determined by the presence or absence of resources,
17 the consumer populations can either undergo cyclic dynamics or
18 reach a steady state. We obtain strong constraints on starvation
19 and recovery rates by deriving allometric scaling relationships
20 and find that population dynamics subject to these constraints
21 can approach the cyclic regime but are typically driven to a steady
22 state. Moreover, we find that these rates fall within a ‘refuge’ in pa-
23 rameter space, where the probability of extinction of the consumer
24 population is minimized. Thus we identify a potential mechanism
25 that may both drive and constrain the dynamics of animal pop-
26ulations. Our model provides a natural framework that predicts
27 maximum body size for mammals by determining the relative sta-
28 bility of an otherwise homogeneous population to a mutant pop-
29 ulation with altered percent body fat. For body masses $\lesssim 10^7$ g,
30 individuals with increased energetic reserves can invade resident
31 populations, and vice versa for body mass $\gtrsim 10^7$ g, thus providing
32 a principled mechanism for a within-lineage driver of Cope’s rule.

33 foraging | starvation | reproduction

34 **Significance Statement** Energetic investment in somatic mainte-
35 nance and growth vs. reproduction directly impacts the dynamics of
36 populations among species. Here, we construct a Nutritional State-
37 structured Model (NSM) to assess the population-level effects of star-
38 vation and recovery of a consumer population in a resource-limited en-
39 vironment, and use allometric scaling relationships for mammals to es-
40 tablish all timescales and rates. Our model reveals that mammalian
41 energetic rates minimize the probability of stochastic extinction, estab-
42 lishes dynamic bounds on mammalian body size while providing inde-
43 pendent theoretical support for the energy equivalence hypothesis, and
44 provides a mechanistic driver for the evolutionary trend towards larger
45 body size known as Cope’s rule.

46 Introduction

47 The behavioral ecology of all organisms is influenced by the en-
48 ergic state of individuals, which directly influences how they
49 invest reserves in uncertain environments. Such behaviors are
50 generally manifested as tradeoffs between investing in somatic
51 maintenance and growth, or allocating energy towards repro-
52 duction [1, 2, 3]. The timing of these behaviors responds to
53 selective pressure, as the choice of the investment impacts fu-
54 ture fitness [4, 5, 6]. The influence of resource limitation on an
55 organism’s ability to maintain its nutritional stores may lead to
56 repeated delays or shifts in reproduction over the course of an
57 organism’s life.

58 The balance between (a) somatic growth and maintenance,
59 and (b) reproduction depends on resource availability [7]. For
60 example, reindeer invest less in calves born after harsh win-
61 ters (when the mother’s energetic state is depleted) than in
62 calves born after moderate winters [8]. Many bird species in-
63 vest differently in broods during periods of resource scarcity

64 compared to normal periods [9, 10], sometimes delaying or even
65 foregoing reproduction for a breeding season [1, 11, 12]. Even
66 freshwater and marine zooplankton have been observed to avoid
67 reproduction under nutritional stress [13], and those that do
68 reproduce have lower survival rates [2]. Organisms may also
69 separate maintenance and growth from reproduction over space
70 and time: many salmonids, birds, and some mammals return to
71 migratory breeding grounds to reproduce after one or multiple
72 seasons in resource-rich environments where they accumulate
73 nutritional reserves [14, 15, 16].

74 Physiology also plays an important role in regulating re-
75 productive expenditures during periods of resource limitation.
76 The data collected thus far has shown that diverse mammals (47
77 species in 10 families) exhibit delayed implantation, whereby fe-
78 males postpone fetal development (blastocyst implantation) un-
79 til nutritional reserves can be accumulated [17, 18]. Many other
80 many species (including humans) suffer irregular menstrual cy-
81 cling and higher abortion rates during periods of nutritional
82 stress [19, 20]. In the extreme case of unicellular organisms,
83 nutrition is unavoidably linked to reproduction because the nu-
84 tritional state of the cell regulates all aspects of the cell cycle
85 [21]. The existence of so many independently evolved mech-
86 anisms across such a diverse suite of organisms highlights the im-
87 portance and universality of the fundamental tradeoff between
88 somatic and reproductive investment. However the general dy-
89 namic implications of these constraints are unknown.

90 Though straightforward conceptually, incorporating the en-
91 ergic dynamics of individuals [22] into a population-level
92 framework [22, 23] presents numerous mathematical obsta-
93 cles [24]. An alternative approach involves modeling the
94 macroscale relations that guide somatic versus reproductive
95 investment in a consumer-resource system. For example,
96 macroscale Lotka-Volterra models assume that the growth rate
97 of the consumer population depends on resource density, thus
98 implicitly incorporating the requirement of resource availability
99 for reproduction [25].

100 In this work, we adopt an alternative approach in which we
101 explicitly account for resource limitation and the subsequent
102 effects of starvation. Namely, only individuals with sufficient
103 energetic reserves can reproduce. Such a constraint leads to
104 reproductive time lags due to some members of the population
105 going hungry and then recovering. Additionally, we incorporate
106 the idea that reproduction is strongly constrained allometrically
107 [3], and is not generally linearly related to resource density. As
108 we shall show, these constraints influence the ensuing popula-

Reserved for Publication Footnotes

109 tion dynamics in dramatic ways.

110 111 Nutritional state-structured model (NSM)

112 We begin by defining a minimal Nutritional State-structured
113 population Model (NSM), where the consumer population is
114 partitioned into two states: (a) an energetically replete (full)
115 state F , where the consumer reproduces at a constant rate λ
116 and does not die from starvation, and (b) an energetically de-
117 ficient (hungry) state H , where the consumer does not repro-
118 duce but dies by starvation at rate μ . The underlying resource
119 R evolves by logistic growth with an intrinsic growth rate α
120 and a carrying capacity equal to one. Consumers transition
121 from the full state F to the hungry state H at a rate σ —the
122 starvation rate—and also in proportion to the absence of re-
123 sources $(1 - R)$. Conversely, consumers recover from state H
124 to state F at rate ρ and in proportion to R . Resources are
125 also eaten by the consumers—at rate ρ by hungry consumers
126 and at rate $\beta < \rho$ by full consumers. This inequality accounts
127 for hungry consumers requiring more resources to replace lost
128 body tissue. The NSM represents a fundamental extension of
129 the idealized starving random walk model of foraging, which
130 focuses on resource depletion, to include reproduction and re-
131 source replenishment [26, 27, 28].

In the mean-field approximation, in which the consumers
and resources are perfectly mixed, their densities evolve accord-
ing to the rate equations

$$\begin{aligned}\dot{F} &= \lambda F + \rho RH - \sigma(1 - R)F, \\ \dot{H} &= \sigma(1 - R)F - \rho RH - \mu H, \\ \dot{R} &= \alpha R(1 - R) - R(\rho H + \beta F).\end{aligned}$$

132 Notice that the total consumer density $F + H$ evolves accord-
133 ing to $\dot{F} + \dot{H} = \lambda F - \mu H$. This resembles the equation of
134 motion for the predator density in the classic Lotka-Volterra
135 model [29], except that the resource density does not appear in
136 the growth term. As discussed above, the attributes of repro-
137 duction and mortality have been explicitly apportioned to the
138 full and hungry consumers, respectively, so that the growth in
139 the total density is decoupled from the resource density.

Equation [1] has three fixed points: two trivial fixed points
at $(F^*, H^*, R^*) = (0, 0, 0)$ and $(0, 0, 1)$, and one non-trivial,
internal fixed point at

$$\begin{aligned}F^* &= \frac{\alpha\lambda\mu(\mu + \rho)}{(\lambda\rho + \mu\sigma)(\lambda\rho + \mu\beta)}, \\ H^* &= \frac{\alpha\lambda^2(\mu + \rho)}{(\lambda\rho + \mu\sigma)(\lambda\rho + \mu\beta)}, \\ R^* &= \frac{\mu(\sigma - \lambda)}{\lambda\rho + \mu\sigma}.\end{aligned}$$

140 The stability of this fixed point is determined by the Jaco-
141 bian matrix \mathbf{J} , where each matrix element $J_{ij} = \partial\dot{X}_i/\partial X_j$
142 when evaluated at the internal fixed point, and \mathbf{X} is the vec-
143 tor (F, H, R) . The parameters in Eq. [1] are such that the
144 real part of the largest eigenvalue of \mathbf{J} is negative, so that the
145 system is stable with respect to small perturbations from the
146 fixed point. Because this fixed point is unique, it is the global
147 attractor for all population trajectories for any initial condition
148 where the resource and consumer densities are both nonzero.

149 From Eq. [2], an obvious constraint on the NSM is that
150 the reproduction rate λ must be less than the starvation rate
151 σ , so that R^* is positive. In fact, when the resource density
152 $R = 0$, the rate equation for F gives exponential growth of
153 F for $\lambda > \sigma$. The condition $\sigma = \lambda$ represents a transcritical
154 (TC) bifurcation [30] that demarcates the physical regime from
155 the unphysical regime where F would grow exponentially with

156 time. The biological implication of the constraint $\lambda < \sigma$ has a
157 simple interpretation—the rate at which a macroscopic organ-
158 ism loses mass due to lack of resources is generally much faster
159 than the rate of reproduction. As we will discuss below, this
160 inequality is a natural consequence of allometric constraints [3]
161 for organisms within empirically observed body size ranges.

162 In the physical regime of $\lambda < \sigma$, the fixed point [2] may
163 either be a stable node or a limit cycle (Fig. 1). In continuous-
164 time systems, a limit cycle arises when a pair of complex con-
165 jugate eigenvalues crosses the imaginary axis to attain positive
166 real parts [31]. This Hopf bifurcation is defined by $\text{Det}(\mathbf{S}) = 0$,
167 with \mathbf{S} the Sylvester matrix, which is composed of the coef-
168 ficients of the characteristic polynomial of the Jacobian ma-
169 trix [32]. As the system parameters are tuned to be within the
170 stable regime but close to the Hopf bifurcation, the amplitude of
171 the transient but decaying cycles become large. Given that eco-
172 logical systems are constantly being perturbed [33], the onset of
173 transient cycles, even though they decay with time in the mean-
174 field description, can increase the extinction risk [34, 35, 36].
175 Thus the distance of a system from the Hopf bifurcation pro-
176 vides a measure of its persistence.

177 When the starvation rate $\sigma \gg \lambda$, a substantial fraction
178 of the consumers are driven to the hungry non-reproducing
179 state. Because reproduction is inhibited, there is a low steady-
180 state consumer density and a high steady-state resource den-
181 sity. However, if $\sigma/\lambda \rightarrow 1$ from above, the population is
182 overloaded with energetically-replete (reproducing) individuals,
183 thereby promoting oscillations between the consumer and re-
184 source densities (Fig. 1).

185 Whereas the relation between consumer growth rate λ and
186 the starvation rate σ defines an absolute bound of biological
187 feasibility—the TC bifurcation— σ also determines the sensitiv-
188 ity of the consumer population to changes in resource density.
189 When $\sigma \gg \lambda$, the steady-state population density is small,
190 thereby increasing the risk of stochastic extinction. On the
191 other hand, as σ decreases, the system will ultimately be poised
192 either near the TC or the Hopf bifurcation (Fig. 1). If the re-
193 covery rate ρ is sufficiently small, the TC bifurcation is reached
194 and the resource eventually is eliminated. If ρ exceeds a thresh-
195 old value, cyclic dynamics will develop as the Hopf bifurcation
196 is approached.

197 198 Role of allometry

199 While there are no a priori constraints on the parameters in
200 the NSM, most organisms correspond to restricted portions of
201 the parameter space. Here we use allometric scaling relations
202 to constrain the covariation of rates in a principled and biologi-
203 cally meaningful manner. Allometric scaling relations highlight
204 common constraints and average trends across large ranges in
205 body size and species diversity. Many of these relations can be
206 derived from a small set of assumptions and below we describe a
207 framework to determine the covariation of timescales and rates
208 across the range of mammals for each of the key parameters of
209 our model (cf. [37]). We are thereby able to define the regime of
210 dynamics occupied by the entire class of mammals along with
211 the key differences between the largest and smallest mammals.

212 Nearly all of the rates described in the NSM are determined
213 by consumer metabolism, which can be used to describe a vari-
214 ety of organismal features [38]. The scaling relation between an
215 organism's metabolic rate B and its body mass M at reproduc-
216 tive maturity is known to scale as $B = B_0 M^\eta$ [39], where the
217 scaling exponent η is typically close to 2/3 or 3/4 for metazoans
218 (e.g., [38]), and has taxonomic shifts for unicellular species be-
219 tween $\eta \approx 1$ in eukaryotes and $\eta \approx 1.76$ in bacteria [40, 3]. An
220 organism's metabolic rate B is proportional to the cost of tis-
221 sue maintenance in the absence of growth (i.e., when the body
222 mass is M). By definition $B = \beta/\xi$, where β is the rate at

which resources are consumed for full consumers (see Eq. [1]) that an organism must meet its maintenance requirements using and where ξ is related to the conversion efficiency of resource the digestion of existing mass as the sole energy source. This to consumer tissue (Supporting Information). assumption implies the following simple metabolic balance

Several efforts have shown how a partitioning of B between growth and maintenance purposes can be used to derive a general equation for both the growth trajectories and growth rates of organisms ranging from bacteria to metazoans [41, 42, 43, 44, 3]. This relation is derived from the simple balance condition [41, 42, 43, 44, 3]

$$B_0 m^\eta = E_m \dot{m} + B_m m,$$

where E_m is the energy needed to synthesize a unit of mass, B_m is the metabolic rate to support an existing unit of mass, and m is the mass of the organism at any point in its development. This balance has the general solution [45, 3]

$$\left(\frac{m(t)}{M}\right)^{1-\eta} = 1 - \left[1 - \left(\frac{m_0}{M}\right)^{1-\eta}\right] e^{-a(1-\eta)t/M^{1-\eta}} \quad [4]$$

where, for $\eta < 1$, $M = (B_0/B_m)^{1/(1-\eta)}$ is the asymptotic mass, $a = B_0/E_m$, and m_0 is mass at birth. We now use this solution to define the timescale of reproduction and recovery from starvation (Fig. 2; see [42] for a detailed presentation of these timescales). The time that it takes to reach a particular mass ϵM is given by the timescale

$$\tau(\epsilon) = \ln \left[\frac{1 - (m_0/M)^{1-\eta}}{1 - \epsilon^{1-\eta}} \right] \frac{M^{1-\eta}}{a(1-\eta)} \quad [5]$$

where we will define values of ϵ to describe a set of rates within our model. For the time to reproduce, $t_\lambda = \tau(\epsilon_\lambda)$, where ϵ_λ is the fraction of the asymptotic mass where an organism is reproductively mature and should be close to one (typically $\epsilon_\lambda \approx 0.95$). The growth rate is then given by $\lambda = \ln(v)/t_\lambda$ where v is the number of offspring produced, and for any constant value of ϵ_λ this will scale like $\lambda \propto M^{\eta-1}$ for $M \gg m_0$ [41, 42, 43, 44, 3].

The rate of recovery $\rho = 1/t_\rho$ requires that an organism accrues sufficient tissue to transition from the hungry to the full state. Since only certain tissues can be digested for energy (for example the brain cannot be degraded to fuel metabolism), we define the rates for starvation, death, and recovery by the timescales required to reach, or return from, specific fractions of the replete-state mass (Fig. 3; see Supporting Information, Table I for parameterizations). We define $m_\sigma = \epsilon_\sigma M$, where $\epsilon_\sigma < 1$ is the fraction of replete-state mass where reproduction ceases. This fraction will be modified if tissue composition systematically scales with adult mass. For example, making use of the observation that body fat in mammals scales with overall body size according to $M_{\text{fat}} = f_0 M^\gamma$ and assuming that once this mass is fully digested the organism starves, this would imply that $\epsilon_\sigma = 1 - f_0 M^\gamma/M$. It follows that the recovery timescale, t_ρ , is the time to go from $m = \epsilon_\sigma \epsilon_\lambda M$ to $m = \epsilon_\lambda M$ (Fig. 2). Using Eqs. [4] and [5] this timescale is given by simply considering an adjusted starting mass of $m'_0 = \epsilon_\sigma \epsilon_\lambda M$, in which case

$$t_\rho = \ln \left[\frac{1 - (\epsilon_\sigma \epsilon_\lambda)^{1-\eta}}{1 - \epsilon^{1-\eta}} \right] \frac{M^{1-\eta}}{a'(1-\eta)} \quad [6]$$

where $a' = B_0/E'_m$ accounts for possible deviations in the biosynthetic energetics during recovery (see Supporting Information). It should be noted that more complicated ontogenetic models explicitly handle storage [44], whereas this feature is implicitly covered by the body fat scaling in our framework.

To determine the starvation rate, σ , we are interested in the time required for an organism to go from a mature adult that reproduces at rate λ , to a reduced-mass hungry state where reproduction is impossible. For starving individuals we assume

or

$$\dot{m}E'_m = -B_m m \quad [7]$$

$$\dot{m} = -\frac{a'}{M^{1-\eta}} m \quad [8]$$

[3] where E'_m is the amount of energy stored in a unit of existing body mass which differs from E_m , the energy required to synthesize a unit of biomass [44]. Given the replete mass, M , of an organism, the above energy balance prescribes the mass trajectory of a non-consuming organism:

$$m(t) = M e^{-a't/M^{1-\eta}}. \quad [9]$$

[286] The time scale for starvation is given by the time it takes $m(t)$ to reach $\epsilon_\sigma M$, which gives

$$t_\sigma = -\frac{M^{1-\eta}}{a'} \ln(\epsilon_\sigma). \quad [10]$$

[288] The starvation rate is then $\sigma = 1/t_\sigma$, which scales with replete-state mass as $1/M^{1-\eta} \ln(1 - f_0 M^\gamma/M)$. An important feature is that σ does not have a simple scaling dependence on λ (Fig. 3), which is important for the dynamics that we later discuss.

[291] The time to death should follow a similar relation, but defined by a lower fraction of replete-state mass, $m_\mu = \epsilon_\mu M$.

[294] Suppose, for example, that an organism dies once it has digested all fat and muscle tissues, and that muscle tissue scales with body mass according to $M_{\text{musc}} = u_0 M^\zeta$. This gives $\epsilon_\mu = 1 - (f_0 M^\gamma + u_0 M^\zeta)/M$. Muscle mass has been shown to be roughly proportional to body mass [46] in mammals and thus ϵ_μ is merely ϵ_σ minus a constant. The time to death is the total time to reach $\epsilon_\mu M$ minus the time to starve, or

$$t_\mu = -\frac{M^{1-\eta}}{a'} \ln(\epsilon_\mu) - t_\sigma, \quad [11]$$

[301] and $\mu = 1/t_\mu$.

[302] Although the rate equations [1] are general, here we focus on parameterizations for terrestrial-bound endotherms, specifically mammals, which range from a minimum of $M \approx 1\text{g}$ (the Etruscan shrew *Suncus etruscus*) to a maximum of $M \approx 10^7\text{g}$ (the late Eocene to early Miocene Indricotheriinae). Investigating other classes of organisms would simply involve altering the metabolic exponents and scalings associate with ϵ . Moreover, we emphasize that our allometric equations describe mean relationships, and do not account for the (sometimes considerable) variance associated with individual species.

312 Stabilizing effects of allometric constraints

[314] As the allometric derivations of the NSM rate laws reveal, starvation and recovery rates are not independent parameters, and the biologically relevant portion of the phase space shown in Fig. 1 is constrained via covarying parameters. Given the parameters of terrestrial endotherms, we find that the starvation rate σ and the recovery rate ρ are constrained to lie within a

[320] small window of potential values (Fig. 4) for the known range of body sizes M . We thus find that the dynamics for all mammalian body sizes is confined to the steady-state regime of the NSM and that limit-cycle behavior is precluded. Moreover, for larger M , the distance to the Hopf bifurcation increases, while

[326] uncertainty in allometric parameters (20% variation around the mean; Fig. 4) results in little qualitative difference in the distance to the Hopf bifurcation. These results suggest that small mammals are more prone to population oscillations—both

stable limit cycles and transient cycles—than mammals with larger body size. Thus our NSM model predicts that population cycles should be less common for larger species and more common for smaller species, particularly in environments where resources are limiting.

It should be noted that previous studies have used allometric constraints to explain the periodicity of cyclic populations [47, 48, 49], suggesting a period $\propto M^{0.25}$. However this relation seems to hold only for some species [50], and potential drivers range from predator and/or prey lifespans to competitive dynamics [51, 52]. Statistically significant support for the existence of population cycles among mammals is predominantly based on time series for small mammals [53], in agreement with our predictions of more pronounced transient dynamics, given how close these points are to the Hopf bifurcation. On the other hand, the longer gestational times and the increased difficulty in measurements, precludes obtaining similar-quality data for larger organisms.

Extinction risk

Within our model, higher rates of starvation result in a larger flux of the population to the hungry state. In this state reproduction is absent, thus increasing the likelihood of extinction. From the perspective of population survival, it is the rate of starvation relative to the rate of recovery that determines the long-term dynamics of the various species (Fig. 1). We therefore examine the competing effects of cyclic dynamics vs. changes in steady state density on extinction risk as a function of σ and ρ . To this end, we computed the probability of extinction, where we define extinction as a population trajectory falling below one tenth of the allometrically constrained steady state at any time between $t = 10^5$ and $t \leq 10^8$. This procedure is repeated for 1000 replicates of the continuous-time system shown in Eq. 1 for an organism of $M = 100$ grams. In each replicate the initial densities are chosen to be $A(F^*, H^*, R^*)$, with A a random variable that is uniformly distributed in $[0, 2]$. By allowing the rate of starvation to vary, we assessed extinction risk across a range of values for σ and ρ between ca. 10^{-6} to 10^{-1} . As expected, higher rates of extinction correlate with both high values of σ if ρ is small, and high values of ρ if σ is small. For low values of σ and high values of ρ , the increased extinction risk results from transient cycles with larger amplitudes as the system nears the Hopf bifurcation (Fig. 5). For high values of σ and low values of ρ , higher extinction risk arises because of the decrease in the steady state consumer population density (Figs. 1B, 5). This interplay creates an ‘extinction refuge’, such that for a constrained range of σ and ρ , extinction probabilities are minimized.

We find that the allometrically constrained values of σ and ρ fall squarely within the extinction refuge (Fig. 5, white point). These values are close enough to the Hopf bifurcation to avoid low steady state densities, and far enough away to avoid large-amplitude transient cycles. The fact that allometric values of σ and ρ fall within this relatively small window supports the possibility that a selective mechanism has constrained the physiological conditions that drive starvation and recovery rates within populations. Such a mechanism would select for organism physiology that generates appropriate σ and ρ values that serve to minimize extinction risk. This selection could occur via the tuning of body fat percentages, metabolic rates, and biomass maintenance efficiencies. To summarize, our finding that the allometrically-determined parameters fall within this low extinction probability region suggests that the NSM dynamics may both drive—and constrain—natural animal populations.

Dynamic and energetic barriers to body size
Metabolite transport constraints are widely thought to place strict boundaries on biological scaling [54, 55, 38] and thereby lead to specific predictions on the minimum possible body size for organisms [56]. Above this bound, a number of energetic and evolutionary mechanisms have been explored to assess the costs and benefits associated with larger body masses, particularly for mammals. One important such example is the *fasting endurance hypothesis*, which contends that larger body size, with consequent lower metabolic rates and increased ability to maintain more endogenous energetic reserves, may buffer organisms against environmental fluctuations in resource availability [57]. Over evolutionary time, terrestrial mammalian lineages show a significant trend towards larger body size (known as Cope’s rule) [58, 59, 60, 61], and it is thought that within-lineage drivers generate selection towards an optimal upper bound of roughly 10^7 grams [58], a value that is likely limited by higher extinction risk for large taxa over longer timescales [59]. These trends are thought to be driven by a combination of climate change and niche availability [61]; however the underpinning energetic costs and benefits of larger body sizes, and how they influence dynamics over ecological timescales, have not been explored. We argue that the NSM provides a suitable framework to explore these issues.

The NSM correctly predicts that species with smaller masses have larger steady-state population densities (Fig. 6A). Moreover, we show that the NSM provides independent theoretical support for the energy equivalence hypothesis [62, 63]. The energy equivalence hypothesis argues that the total energy use, B_{tot} , of a population is constant independent of species size (e.g. [62, 63]). This hypothesis is based on observations showing that the abundance, N , of a species is proportional to the inverse of individual metabolism (e.g. $N \propto M^{-3/4}/B_0$) (e.g. [62, 63]). This is usually stated as $B_{tot} = NB = C$ where C is a constant, and has been shown to hold in both mammalian and vascular plant communities [62, 63]. Figure 6A shows that both F^* and H^* scale like $M^{-\eta}$ over a wide range of organism sizes and Figure 6B shows that F^*B is relatively constant over this same range. This result is remarkable because it illustrates that the steady state values of the NSM combined with the derived timescales naturally give rise to the energy equivalence result. Our model shows that the equivalence breaks down at both the minimum and maximum observed body sizes for mammals, suggesting that these are hard limits where deviations outside of this range are energetically suboptimal. Significant deviations from constant energy use occur at $M \lesssim 1$ at the small end of the mammalian range and $M \approx 6.5 * 10^7$ at the large end.

We contend that the NSM provides a mechanistic understanding of the energetic dynamics that give rise to both observed limitations on mammalian body size as well as the observed trend towards larger body size over evolutionary time. The NSM predicts that the steady state resource density R^* decreases with increasing body size of the consumer population (Fig. 6C), and classic resource competition theory predicts that the species surviving on the lowest resource abundance will outcompete others [64, 65, 66]. Thus, the combined NSM steady-state dynamics and allometric timescales predict that larger mammals have an intrinsic competitive advantage given a common resource, but does not offer a within-lineage mechanism by which larger body sizes are selected for.

To examine whether the NSM could provide such a mechanism, we begin by noting that a theoretical upper bound on mammalian body size is given by $\epsilon_\sigma = 0$, where mammals are entirely composed of metabolic reserves, and this occurs at $M = 8.3 \times 10^8$, or $4.5 \times$ the mass of a blue whale. Next we examine to what extent a more realistic upper bound to body mass may serve as an evolutionary attractor, thus provid-

ing a suitable within-linneage mechanism for Cope's rule. We directly assess the susceptibility of an otherwise homogeneous population to invasion by a mutated subset of the population (denoted by ') where individuals have a modified proportion of body fat $M' = M(1 + \chi)$ where $\chi \in [-1, 1]$, thus altering the rates of starvation $\sigma(M')$, recovery $\rho(M')$, and maintenance $\beta(M')$. There is no internal fixed point corresponding to a state where both original residents and invaders coexist (except for the trivial state $\chi = 0$). To assess the susceptibility to invasion as a function of the invader mass, we determine which consumer has a higher steady-state density for a given value of χ . We find that for $1 \leq M < 8.43 \times 10^6$ g, having additional body fat ($\chi > 0$) results in a higher steady-state invader population density ($H'^* + F'^* > H^* + F^*$). Thus the invader has an intrinsic advantage over the resident population. However, for $M > 8.43 \times 10^6$ leaner individuals ($\chi < 0$) have advantageous steady state densities.

The observed switch in susceptibility as a function of χ at $M_{\text{opt}} = 8.43 \times 10^6$ thus serves as an attractor, or an unavoidable evolutionary stable state, such that the NSM predicts organismal mass to increase if $M < M_{\text{opt}}$ and decrease if $M > M_{\text{opt}}$. Moreover, M_{opt} , which is entirely determined by the population-level consequences of energetic constraints, is remarkably close to the maximum body size observed in the North American mammalian fossil record [58] as well as the mass dictated from an evolutionary model of body size evolution [59].

While the state of the environment, as well as the competitive landscape, will determine whether specific body sizes are selected for or against [61], we suggest that the dynamics of starvation and recovery described in the NSM may provide a general driving mechanism for the evolution of larger body size among terrestrial mammals. The energetics associated with somatic maintenance, growth, and reproduction are important elements that influence the dynamics of all populations [11]. The NSM is a minimal and general model that incorporates the dynamics of starvation and recovery that are expected to occur in resource-limited environments. By incorporating allometric relations between the rates in the NSM, we found: (i) different organismal masses have distinct population dynamic regimes, (ii) allometrically-intrinsic advantage over the resident population. However, for determined rates of starvation and recovery appear to minimize extinction risk, and (iii) the dynamic consequences of these rates may introduce additional drivers and hard bounds.

The observed switch in susceptibility as a function of χ arises on the evolution of minimum and maximum body size. We suggest that the NSM offers a means by which the dynamics of energetic constraints can be assessed using macroscale interactions between and among species. Future efforts will involve exploring the consequences of these dynamics in a spatially explicit framework, thus incorporating elements such as movement costs and spatial heterogeneity, which may elucidate additional tradeoffs associated with the dynamics of starvation and recovery.

- 512 1. Martin TE (1987) Food as a Limit on Breeding Birds: A Life-History Perspective. *Annu. Rev. Ecol. Syst.* 18:453–487.
- 513 2. Kirk KL (1997) Life-History Responses to Variable Environments: Starvation and Reproduction in Planktonic Rotifers. *Ecology* 78:434–441.
- 514 3. Kempes CP, Dutkiewicz S, Follows MJ (2012) Growth, metabolic partitioning, and the size of microorganisms. *PNAS* 109:495–500.
- 515 4. Mangel M, Clark CW (1988) *Dynamic Modeling in Behavioral Ecology* (Princeton University Press, Princeton).
- 516 5. Mangel M (2014) Stochastic dynamic programming illuminates the link between environment, physiology, and evolution. *B. Math. Biol.* 77:857–877.
- 517 6. Yeakel JD, Dominy NJ, Koch PL, Mangel M (2014) Functional morphology, stable isotopes, and human evolution: a model of consilience. *Evolution* 68:190–203.
- 518 7. Morris DW (1987) Optimal Allocation of Parental Investment. *Oikos* 49:332.
- 519 8. Tveraa T, Fauchald P, Henaug C, Yoccoz NG (2003) An examination of a compensatory relationship between food limitation and predation in semi-domestic reindeer. *Oecologia* 137:370–376.
- 520 9. Daan S, Dijkstra C, Drent R, Meijer T (1988) Food supply and the annual timing of avian reproduction.
- 521 10. Jacot A, Valcu M, van Oers K, Kempenaers B (2009) Experimental nest site limitation affects reproductive strategies and parental investment in a hole-nesting passerine. *Animal Behaviour* 77:1075–1083.
- 522 11. Stearns SC (1989) Trade-Offs in Life-History Evolution. *Funct. Ecol.* 3:259.
- 523 12. Barboza P, Jorde D (2002) Intermittent fasting during winter and spring affects body composition and reproduction of a migratory duck. *J Comp Physiol B* 172:419–434.
- 524 13. Threlkeld ST (1976) Starvation and the size structure of zooplankton communities. *Freshwater Biol.* 6:489–496.
- 525 14. Weber TP, Ens BJ, Houston AI (1998) Optimal avian migration: A dynamic model of fuel stores and site use. *Evolutionary Ecology* 12:377–401.
- 526 15. Mduma SAR, Sinclair ARE, Hilborn R (1999) Food regulates the Serengeti wildebeest: a 40-year record. *J. Anim. Ecol.* 68:1101–1122.
- 527 16. Moore JW, Yeakel JD, Peard D, Lough J, Beere M (2014) Life-history diversity and its importance to population stability and persistence of a migratory fish: steelhead in two large North American watersheds. *J. Anim. Ecol.* 83:1035–1046.
- 528 17. Mead RA (1989) in *Carnivore Behavior, Ecology, and Evolution* (Springer US, Boston, MA), pp 437–464.
- 529 18. Sandell M (1990) The Evolution of Seasonal Delayed Implantation. *The Quarterly Review of Biology* 65:23–42.
- 530 19. Bulik CM, et al. (1999) Fertility and Reproduction in Women With Anorexia Nervosa. *J. Clin. Psychiatry* 60:130–135.
- 531 20. Trites AW, Donnelly CP (2003) The decline of Steller sea lions *Eumetopias jubatus* in Alaska: a review of the nutritional stress hypothesis. *Mammal Review* 33:3–28.
- 532 21. Glazier DS (2009) Metabolic level and size scaling of rates of respiration and growth in unicellular organisms. *Funct. Ecol.* 23:963–968.
- 533 22. Kooijman SALM (2000) *Dynamic Energy and Mass Budgets in Biological Systems* (Cambridge).
- 534 23. Sousa T, Domingos T, Poggiale JC, Kooijman SALM (2010) Dynamic energy budget theory restores coherence in biology. *Philos. T. Roy. Soc. B* 365:3413–3428.
- 535 24. Diekmann O, Metz JAJ (2010) How to lift a model for individual behaviour to the population level? *Philos. T. Roy. Soc. B* 365:3523–3530.
- 536 25. Murdoch WW, Briggs CJ, Nisbet RM (2003) *Consumer-resource Dynamics, Monographs in population biology* (Princeton University Press).
- 537 26. Benichou O, Redner S (2014) Depletion-Controlled Starvation of a Diffusing Forager. *arXiv*.
- 538 27. Benichou O, Chupeau M, Redner S (2016) Role of Depletion on the Dynamics of a Diffusing Forager.
- 539 28. Chupeau M, Benichou O, Redner S (2016) Universality classes of foraging with resource renewal. *Phys. Rev. E* 93:032403.
- 540 29. Murray JD (2011) *Mathematical Biology: I. An Introduction*, Interdisciplinary Applied Mathematics (Springer New York, Melaka Manipal Medical College (Manipal Campus), International Centre for Health Sciences, Madhav Nagar, Manipal, Udupi District, Karnataka State, India. nayaksathish@yahoo.com) Vol. 110.
- 541 30. Strogatz SH (2008) *Nonlinear Dynamics and Chaos, With Applications to Physics, Biology, Chemistry, and Engineering* (Westview Press).
- 542 31. Guckenheimer J, Holmes P (1983) *Nonlinear oscillations, dynamical systems, and bifurcations of vector fields* (Springer, New York).
- 543 32. Gross T, Feudel U (2004) Analytical search for bifurcation surfaces in parameter space. *Physica D* 195:292–302.
- 544 33. Hastings A (2001) Transient dynamics and persistence of ecological systems. *Ecol. Lett.* 4:215–220.
- 545 34. Neubert M, Caswell H (1997) Alternatives to resilience for measuring the responses of ecological systems to perturbations. *Ecology* 78:653–665.
- 546 35. Caswell H, Neubert MG (2005) Reactivity and transient dynamics of discrete-time ecological systems. *Journal of Difference Equations and Applications* 11:295–310.
- 547 36. Neubert M, Caswell H (2009) Detecting reactivity. *Ecology*.
- 548 37. Yodzis P, Innes S (1992) Body Size and Consumer-Resource Dynamics. *Am. Nat.* 139:1151–1175.
- 549 38. Brown J, Gillooly J, Allen A, Savage V, West G (2004) Toward a metabolic theory of ecology. *Ecology* 85:1771–1789.
- 550 39. West GB, Woodruff WH, Brown JH (2002) Allometric scaling of metabolic rate from molecules and mitochondria to cells and mammals. *Proc. Natl. Acad. Sci. USA* 99 Suppl 1:2473–2478.
- 551 40. DeLong JP, Okie JG, Moses ME, Sibly RM, Brown JH (2010) Shifts in metabolic scaling, production, and efficiency across major evolutionary transitions of life. *PNAS* 107:12941–12945.
- 552 41. West GB, Brown JH, Enquist BJ (2001) A general model for ontogenetic growth. *Nature* 413:628–631.
- 553 42. Moses ME, et al. (2008) Revisiting a Model of Ontogenetic Growth: Estimating Model Parameters from Theory and Data. <http://dx.doi.org.proxy.lib.sfu.ca/10.1086/679735> 171:632–645.
- 554 43. Gillooly JF, Charnov EL, West GB, Savage VM, Brown JH (2002) Effects of size and temperature on developmental time. *Nature* 417:70–73.
- 555 44. Hou C, et al. (2008) Energy Uptake and Allocation During Ontogeny. *Science* 322:736–739.
- 556 45. Bettencourt LMA, Lobo J, Helbing D, Kuhnert C, West GB (2007) Growth, innovation, scaling, and the pace of life in cities. *Proc. Natl. Acad. Sci. USA* 104:7301–7306.

- 607 46. Folland JP, Mc Cauley TM, Williams AG (2008) Allometric scaling of strength mea- 635 59. Clauset A, Redner S (2009) Evolutionary Model of Species Body Mass Diversifica-
608 surements to body size. *Eur J Appl Physiol* 102:739–745. 636 tion. *Phys. Rev. Lett.* 102:038103.
609 47. Calder III WA (1983) An allometric approach to population cycles of mammals. *J. 637 60. Smith F, Boyer A, Brown J, Costa D (2010) The Evolution of Maximum Body Size of
610 Theor. Biol.* 100:275–282. 638 Terrestrial Mammals. *Science*.
611 48. Peterson RO, PAGE RE, DODGE KM (1984) Wolves, Moose, and the Allometry of 639 61. Saarinen JJ, et al. (2014) Patterns of maximum body size evolution in Cenozoic
612 Population Cycles. *Science* 224:1350–1352. 640 land mammals: eco-evolutionary processes and abiotic forcing. *Proc Biol Sci*
613 49. Krukonis G, Schaffer WM (1991) Population cycles in mammals and birds: Does 641 281:20132049–20132049.
614 periodicity scale with body size? *J. Theor. Biol.* 148:469–493. 642 62. Allen AP, Brown JH, Gillooly JF (2002) Global Biodiversity, Biochemical Kinetics,
615 50. Hendriks AJ, Mulder C (2012) Delayed logistic and Rosenzweig(MacArthur models 643 643 and the Energetic-Equivalence Rule. *Science* 297:1545–1548.
616 with allometric parameter setting estimate population cycles at lower trophic levels 644 63. Enquist BJ, Brown JH, West GB (1998) Allometric scaling of plant energetics and
617 well. *Ecological Complexity* 9:43–54. 645 population density : Abstract : Nature. *Nature* 395:163–165.
618 51. Kendall BE, et al. (1999) Why do populations cycle? A synthesis of statistical and 646 64. Tilman D (1981) Tests of Resource Competition Theory Using Four Species of Lake
619 mechanistic modelling approaches. *Ecology* 80:1789–1805. 647 Michigan Algae. *Ecology* 62:802–815.
620 52. Höglstedt G, Seldal T, Breistol A (2005) Period length in cyclic animal populations. 648 65. Dutkiewicz S, Follows MJ, Bragg JG (2009) Modeling the coupling of ocean ecology
621 *Ecology* 86:373–378. 649 and biogeochemistry. *Global Biogeochem. Cycles* 23:n/a–n/a.
622 53. Kendall, Prendergast, Bjornstad (1998) The macroecology of population dynamics: 650 66. Barton AD, Dutkiewicz S, Flierl G, Bragg J, Follows MJ (2010) Patterns of Diversity
623 taxonomic and biogeographic patterns in population cycles. *Ecol. Lett.* 1:160–164. 651 in Marine Phytoplankton. *Science* 327:1509–1511.
624 54. Brown J, Marquet P, Taper M (1993) Evolution of body size: consequences of an 652
625 energetic definition of fitness. *Am. Nat.* 142:573–584.
626 55. West GB, Brown JH, Enquist BJ (1997) A General Model for the Origin of Allometric 653
627 Scaling Laws in Biology. *Science* 276:122–126.
628 56. West GB, Woodruff WH, Brown JH (2002) Allometric scaling of metabolic rate from 654
629 molecules and mitochondria to cells and mammals. *Proc. Natl. Acad. Sci. USA* 99:2473–2478. 655
631 57. Millar J, Hickling G (1990) Fasting Endurance and the Evolution of Mammalian 656
632 Body Size. *Funct. Ecol.* 4:5–12. 657
633 58. Alroy J (1998) Cope's rule and the dynamics of body mass evolution in North 658
634 American fossil mammals. *Science* 280:731. 659
634

652 **ACKNOWLEDGMENTS.** We thank Luis Bettencourt, Jean Philippe Gibert,
653 Eric Libby, and Seth Newsome for helpful discussions and comments on the
654 manuscript. J.D.Y. was supported by startup funds at the University of California,
655 Merced, and an Omidyar Postdoctoral Fellowship at the Santa Fe Institute. C.P.K.
656 was supported by an Omidyar Postdoctoral Fellowship at the Santa Fe Institute.
657 S.R. was supported by grants DMR-1608211 and 1623243 from the National
658 Science Foundation, and by the John Templeton Foundation, all at the Santa Fe
659 Institute.

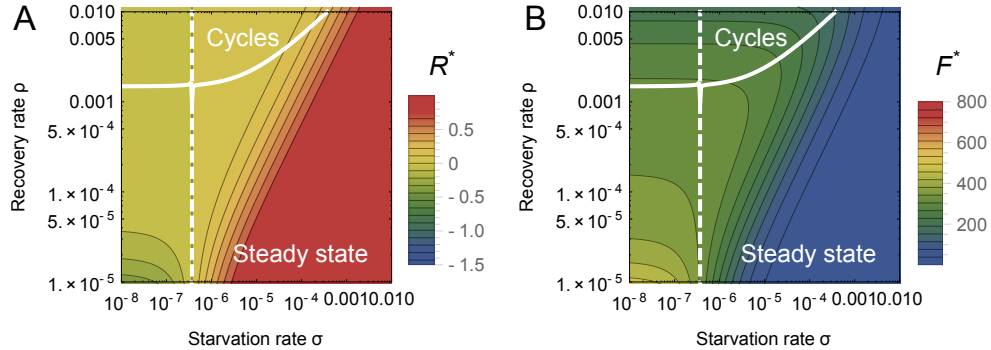


Fig. 1: The transcritical (dashed) and Hopf bifurcation (solid) as a function of the starvation rate σ and recovery rate ρ for a 100g consumer. These bifurcation conditions separate parameter space into infeasible, cyclic, and steady state dynamic regimes. The color gradient shows the steady state densities for (A) the resource R^* and the (B) energetically replete consumers F^* , (warmer colors denote higher densities). Steady state densities for the energetically deficient consumers H^* (not shown) scale with those for F^* .

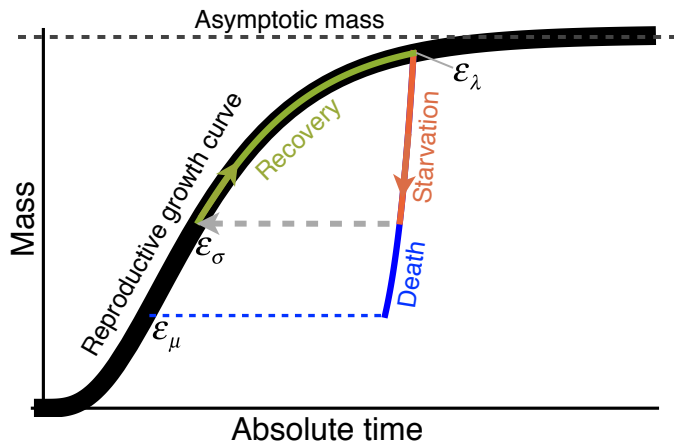


Fig. 2: The growth trajectory over absolute time of an individual organism as a function of body mass. Initial growth follows the black trajectory to an energetically replete reproductive adult mass $m = \epsilon_\lambda M$ which we assume is 95% asymptotic mass M . Starvation follows the red trajectory to $m = \epsilon_\sigma \epsilon_\lambda M$, and recovery follows the green growth trajectory to the replete adult mass. Alternatively, death from starvation follows the blue trajectory to $m = \epsilon_\mu \epsilon_\lambda M$.

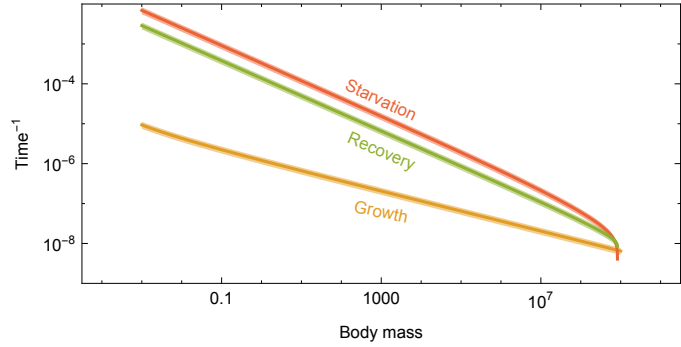


Fig. 3: Allometrically constrained starvation rate σ (red) and recovery rate ρ (green) relative to the reproductive rate λ (orange) as a function of body mass. The rate of starvation is greater than the rate of reproduction for all realized terrestrial endotherm body sizes. Mean values $\pm 20\%$ variation are shown by the shaded region for each rate.

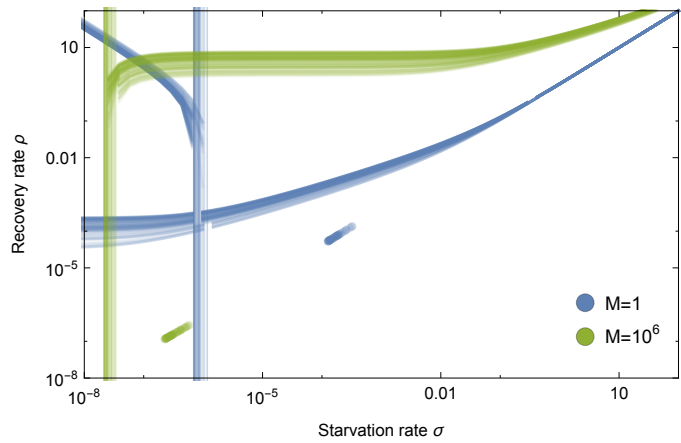


Fig. 4: Transcritical (vertical lines) and Hopf bifurcations (curves) for allometrically determined starvation σ and recovery ρ rates as a function of different mammalian body sizes: $M = A \times 10^1 \text{g}$ (blue) and $M = A \times 10^6 \text{g}$ (green), where A is a random uniform variable in $[1, 9]$. Points denote realized values of σ and ρ given the drawn values for M .

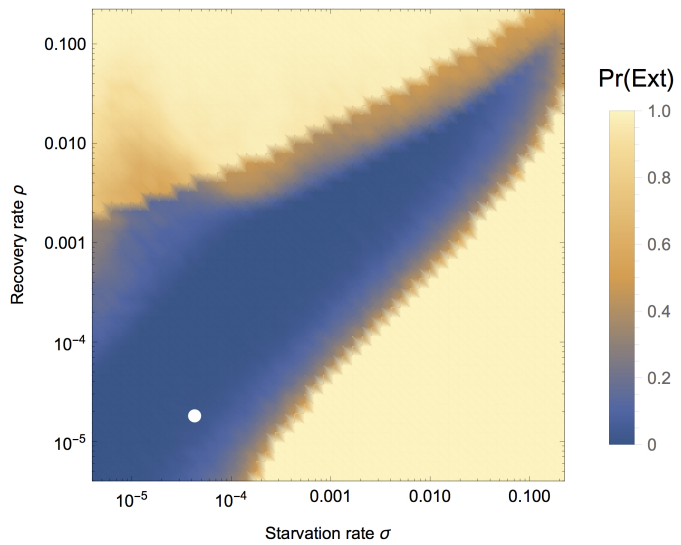


Fig. 5: Probability of extinction for a 100g consumer as a function of the starvation rate σ and recovery rate ρ , where the initial density is given as $A(F^*, H^*, R^*)$, with A being a random uniform variable in $[0, 2]$. Extinction is defined as the population trajectory falling below $0.1 \times$ the allometrically constrained steady state. The white point denotes the allometrically constrained starvation and recovery rate.

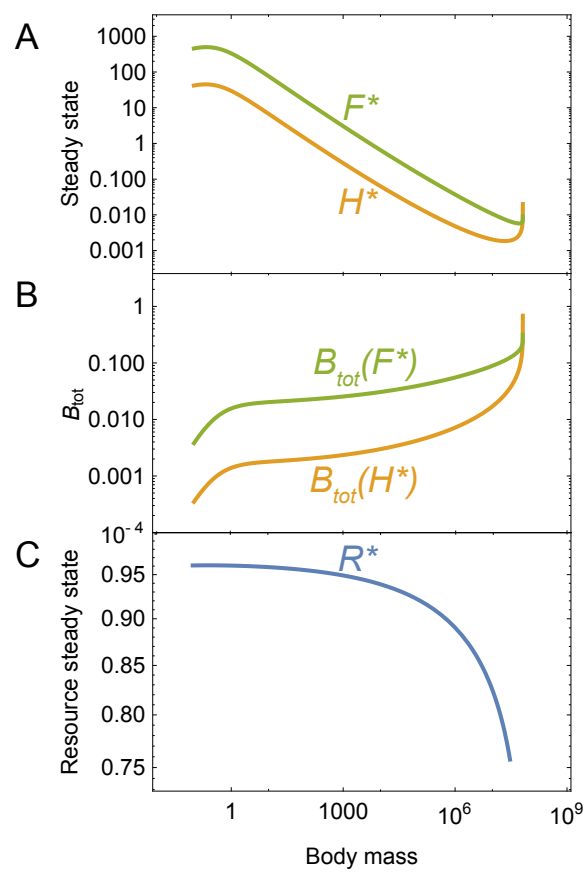


Fig. 6: (A) Consumer steady states F^* (green) and H^* (orange) as a function of body mass. (B) Total energetic use B_{tot} of consumer populations at the steady state as a function of body mass. (C) Resource steady state R^* as a function of consumer body mass.

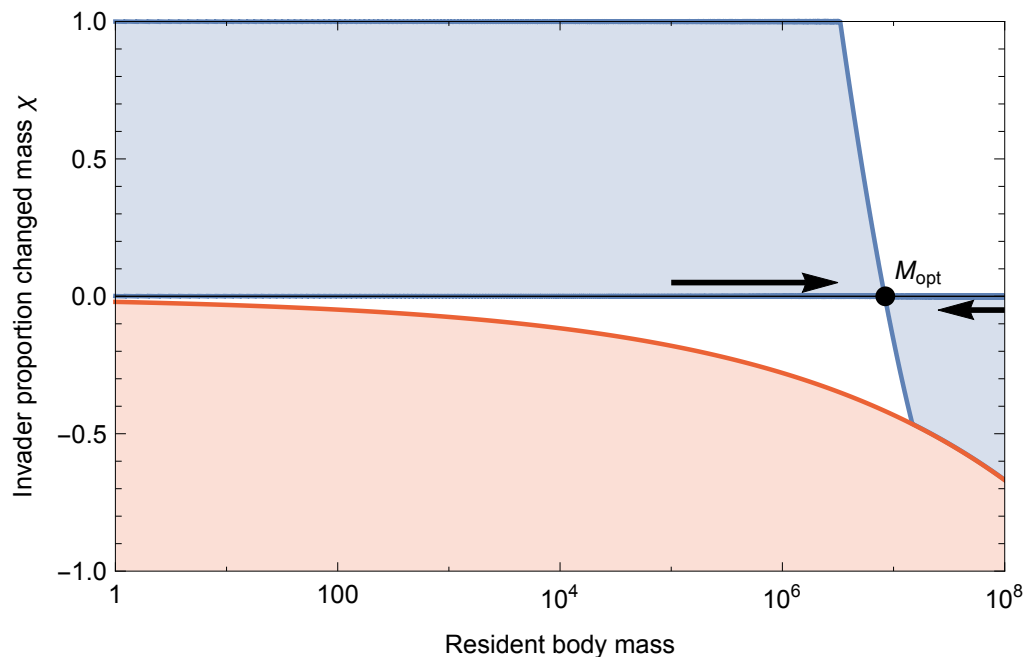


Fig. 7: Invasion feasibility for organisms with a proportional change in mass χ against a population with a resident body mass M . The blue region denotes proportions of modified mass χ resulting in successful invasion. The red region denotes values of χ that result in a mass that is below the starvation threshold and is thus infeasible. Arrows point to the predicted optimal mass $M_{\text{opt}} = 8.43 \times 10^6$, which serves as the unininvadable, evolutionary stable state.

Supporting Information for “The dynamics of starvation and recovery”

1 **Justin D. Yeakel * †‡, Christopher P. Kempes †, and Sidney Redner †§**

4 *School of Natural Science, University of California Merced, Merced, CA, †The Santa Fe Institute, Santa Fe, NM, §Department of Physics, Boston University, Boston
5 MA, and ‡To whom correspondence should be addressed: jdyeakel@gmail.com

6 Submitted to Proceedings of the National Academy of Sciences of the United States of America

7 Parameter Values and Estimates

8 Many of the parameter values employed in our model have ei-
9 ther been directly measured in previous studies or can be esti-
10 mated from combining several previous studies. Here we outline
11 previous measurements and simple estimates of the parameters.

12 **Standard synthesis and metabolic parameters** Metabolic rate has
13 been generally reported to follow an exponent close to $\eta = 0.75$
14 (e.g. [1, 2] and the supplement of [3]). We make this assump-
15 tion in the current paper, although alternate exponents, which
16 are known to vary between roughly 0.25 and 1.5 for single species
17 [2], could be easily incorporated into our framework, and this
18 variation is effectively handled by the 20% variations that we
19 consider around mean trends. It is important to note the expo-
20 nent, because it not only defines several scalings in our frame-
21 work but also the value of the metabolic normalization constant,
22 B_0 , given a set of data. For mammals the metabolic normal-
23 ization constant has been reported to vary between 0.018 (W
24 $g^{-0.75}$) and 0.047 ($W g^{-0.75}$) [3, 1], where the former value rep-
25 resents basal metabolic rate and the latter represents the field
26 metabolic rate. We employ the field metabolic rate for our NSM
27 model which is appropriate for active mammals (Table 1).

28 The energy to synthesize a unit of biomass, E_m , has been
29 reported to vary between 1800 to 9500 ($J g^{-1}$) (e.g. [1, 2, 3]) in
30 mammals with a mean value across many taxonomic groups of
31 5,774 ($J g^{-1}$) [2]. The unit energy available during starvation,
32 E' , could range between 7000 ($J g^{-1}$), the return of the total
33 energy stored during ontogeny [3] to a biochemical upper bound
34 of $E' = 36,000$ ($J g^{-1}$) for the energetics of palmitate [4, 3].
35 For our calculations we use the measured value for bulk tissues
36 of 7000 which assumes that the energy stored during ontogeny
37 is returned during starvation [3].

38 For the scaling of body composition it has been shown that
39 fat mass follows $M_{\text{fat}} = f_0 M^\gamma$, with measured relationships
40 following $0.018M^{1.25}$ [5], $0.02M^{1.19}$ [6], and $0.026M^{1.14}$ [7].
41 We use the values from [6] which falls in the middle of this
42 range. Similarly, the muscle mass follows $M_{\text{musc}} = u_0 M^\zeta$ with
43 $u_0 = 0.383$ and $\zeta = 1.00$ [7].

44 The final parameters that we must consider connect the re-
45 source growth rate to the total metabolic rate of an organism.
46 That is, we are interested in the relative rates of resource re-
47 covery and consumption by the total population. From [8] the

48 total resource use of a population with an individual body size
49 of M is given by $B_{\text{pop}} = 0.00061x^{-0.03}$ ($W m^{-2}$). Considering
50 an energy density of 18200 ($J g^{-1}$) of grass [9] and an NPP
51 between and 1.59×10^{-6} and 7.92×10^{-5} ($g s^{-1} m^{-2}$) would
52 give a range of resource rates between 0.029 and 1.44 ($W m^{-2}$).
53 This gives a ratio of total resource consumption to supply rates
54 between 0.00042 and 0.021, and we used a value of 0.002 in our
55 calculations and simulations.

Table 1: Parameter values for mammals

Parameter	Value	References
η	3/4	(e.g. [1, 2, 3])
E_m	5774 ($J \text{ gram}^{-1}$)	[2, 1, 3]
E'_m	36,000	[4, 3]
B_0	0.047 ($W g^{-0.75}$)	[3]
γ	1.19	[6]
f_0	0.02	[6]
ζ	1.00	[7]
u_0	0.38	[7]

56 **Rate equations for invaders with modified body mass** If an invad-
57 ing subset of the resident population of mass M has an altered
58 mass $M' = M(1 + \chi)$ where χ varies between $[-1, 1]$ ($\chi < 0$
59 denotes a leaner invader; $\chi > 0$ denotes an invader with more
60 endogenous reserves), the invading population will have the fol-
61 lowing modified rates: $\sigma' = \sigma(M')$, $\rho' = \rho(M')$, $\beta' = \beta(M')$.
62 Because we are assuming that the invading population is only
63 modifying its endogenous energetic stores, we assume that the
64 proportion of body mass that is non-adipose tissue remains the
65 same as the resident population. This assumption leads to the
66 following modified timescales:

$$t_{\sigma'} = \frac{-M^{1/4}}{B_0/E'_m} \log \left(\frac{\epsilon_\sigma}{\chi + 1} \right), \quad [1]$$
$$t_{\rho'} = \frac{-4M^{1/4}}{B_0/E'_m} \log \left(\frac{1 - (\epsilon_\lambda(\chi + 1))^{1/4}}{1 - (\epsilon_\lambda\epsilon_\sigma)^{1/4}} \right),$$
$$t_{\beta'} = \xi B_0 (M(\chi + 1))^{3/4}.$$

- 67 1. West GB, Brown JH, Enquist BJ (2001) A general model for ontogenetic growth. *Nature* 413:628–631.
- 68 2. Moses ME, et al. (2008) Revisiting a Model of Ontogenetic Growth: Estimating Model
69 Parameters from Theory and Data. <http://dx.doi.org.proxy.lib.sfu.ca/10.1086/679735>
- 70 71 171:632–645.
- 72 3. Hou C, et al. (2008) Energy Uptake and Allocation During Ontogeny. *Science* 322:736–
73 739.
- 74 4. Stryer L (1995) *Biochemistry, Fourth Edition* (W.H. Freeman and Company, New
75 York), pp 608–611.
- 76 5. Dunbrack RL, Ramsay MA (1993) The Allometry of Mammalian Adaptations to Sea-
77 sonal Environments: A Critique of the Fasting Endurance Hypothesis. *Oikos* 66:336–
78 342.
- 79 6. Lindstedt SL, Boyce MS (1985) Seasonality, Fasting Endurance, and Body Size in
80 Mammals. *Am. Nat.* 125:873–878.
- 81 7. Lindstedt SL, Schaeffer PJ (2002) Use of allometry in predicting anatomical and
82 physiological parameters of mammals. *Lab. Anim.* 36:1–19.
- 83 8. Allen AP, Brown JH, Gillooly JF (2002) Global biodiversity, biochemical kinetics, and
84 the energetic-equivalence rule. *Science* 297:1545–1548.
- 85 9. Estermann BL, Weltstein HR, Sutter F, Kreuzer M (2001) Nutrient and energy con-
86 version of grass-fed dairy and suckler beef cattle kept indoors and on high altitude
87 pasture. *Animal Research* 50:477–493.

Reserved for Publication Footnotes